

One-Dimension Finite Element Modeling of Grouted Ground Anchor

Nadher H. Al-Baghdadi
Department of Civil Engineering
Faculty of Engineering
University of Kufa
Najaf, Iraq
nadhir.albaghdadi@uokufa.edu.iq

Balqees A. Ahmed
Department of Civil Engineering
College of Engineering
University of Baghdad
Baghdad, Iraq
balqees.a@coeng.uobaghdad.edu.iq

Ala N. Al-Jorany
Department of Civil Engineering
College of Engineering
University of Baghdad
Baghdad, Iraq
alaljorany@gmail.com

Received: 11 September 2022 | Revised: 5 October 2022 and 9 October 2022 | Accepted: 10 October 2022

Abstract-In the present research work, a one-dimension finite element model has been developed to simulate both compression and tension types of grouted ground anchors. The steel tendon-grout interface has been modeled by using the local bond-slip model, while the soil-grout interface has been modeled with a series of perfectly elastic plastic springs. The verification of the proposed one-dimension finite element model has been made by comparison of the model results with a three-dimension finite element model developed by commercial finite element software PLAXIS, and with the results of field tests of tension-type grouted ground anchor. A parametric study has been made to study the load-transfer mechanism for both types of anchors, compression, and tension. The compression-type anchor exhibits less displacement than the tension one under the same applied load. The developed strain in the grouted body of the compression-type anchor is much smaller than the tension-type one, regardless of the type of strain.

Keywords-ground anchor; finite element; sandy soil; compression anchor; grout

I. INTRODUCTION

One dimensional finite element modeling has been widely used to model pile foundations with all types of loadings, i.e. axial, lateral, and torsional [1-3]. A pile foundation is modeled by dividing it into a certain number of elements, the type of which depends on the geometry of the problem, loading type, and boundary conditions. Two noded bar elements, with one degree of freedom per node, can be used effectively in axial loading conditions in both compression and tension. The soil resistance is modeled by using linear or nonlinear springs connected to every node. The grouted ground anchor could be modeled by the same method of pile foundation modeling, with adjustments due to differences between the two geotechnical

elements.

Many researchers have used one-dimension finite elements to model the grouted ground anchor. Authors in [4, 5] presented a one-dimensional finite element model of the compression grouted ground anchor pull-out test. Two noded bar elements with one degree of freedom in the axial direction at each node have been used to simulate the grouted body. Since the anchor is a compression type, i.e. the grouted body is always subjected to compression stress, a linear elastic model is used to model the grout. According to the loading mechanism of the compression anchor, the point of load application is located at the bottom node of the grouted body, so the strand has not been involved in the finite element model. The surrounding soil has been simulated by a nonlinear spring model governed by a (t-z) hyperbolic relation. Authors in [6] used a one-dimension finite element to simulate an instrumented field test of grouted ground anchor. Spring elements have been used to model separately the strands and the grout. Along the free length of the anchor, there are no connections between the adjacent nodes of the strand and the grout, while these nodes have been connected along the bonded length of the anchor, to model the bond between the strand and the grout, by using the damage model proposed in [7, 8]. According to it, the interface stiffness decreases as the relative displacement between adjacent nodes of strand and grout increases. The surrounding soil has been modeled by linear elastic springs connected to the nodes of the grout elements. This model was used because the strength of the surrounding soil in the field test has not reached its peak strength. Steel strand behavior has been modeled as linear elastic. The grout under compression has been modeled as linear elastic, while it has been considered to have zero stiffness under tension.

Corresponding author: Nadher H. Al-Baghdadi

II. FINITE ELEMENT MODELING

A finite element model has been developed to simulate the tension-type and the compression-type ground anchors in this work. Two noded rod elements have been used to model the grouted body along the free and bonded lengths. Each node has one degree of freedom in the axial direction. The tendon has been modeled along the bonded length only, by using the same element that has been used to simulate the bonded length of the grouted body. The stiffness of the bar element for both grout and tendon is calculated by using (1) and (2):

$$[K_e]_{grout} = \frac{(EA)_{grout}}{l} \times \begin{bmatrix} 1 & -1 \\ -1 & 1 \end{bmatrix} \quad (1)$$

$$[K_e]_{tendon} = \frac{(EA)_{tendon}}{l} \times \begin{bmatrix} 1 & -1 \\ -1 & 1 \end{bmatrix} \quad (2)$$

where l is the length of the element, E is the modulus of elasticity, and A is the cross-section area respectively, for both grouted body and tendon according to the subscript.

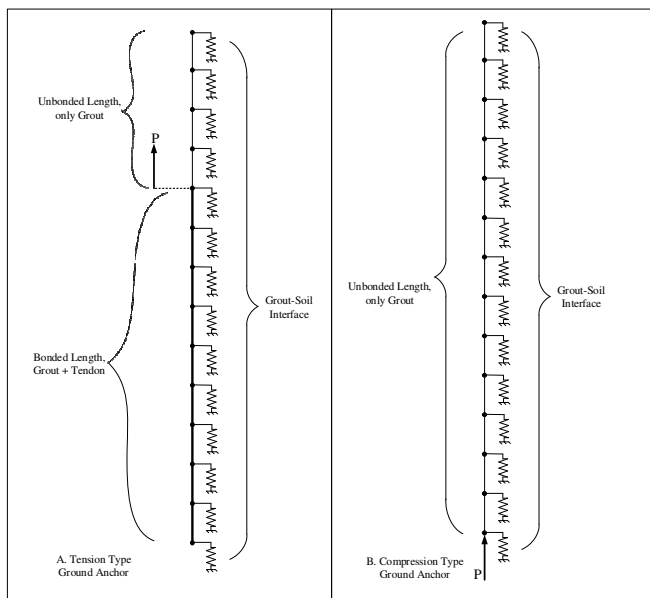


Fig. 1. One-dimensional finite element modelling of ground anchor, A: tension type and B: compression type.

The stiffness of the bonded length is the summation of the stiffnesses of the grout and the tendon, as shown in (3). The tendon along the free length is not considered, as the load application point is located at the top end of the bonded length, for tension anchor type, as shown in Figure 1. For compression-type anchors, the load application point is located at the toe of the anchor, and the total length of the anchor is considered a free length. The stiffness of the element along the free length is only the grout stiffness, as shown in (4). The load is applied at the top node of bonded length in the case of the tension anchor, while the load is applied at the tip node of the anchor model. Figure 1 shows a schematic diagram of the one-dimensional finite element model for tension and compression types of ground anchors.

$$[K_e]_{bonded} = [K]_{grout} + [K]_{tendon} \quad (3)$$

$$[K_e]_{free} = [K]_{grout} \quad (4)$$

A. Soil-Grout Interface Modeling

The interface between soil and grouted body is modeled using a nonlinear spring connected to all the grouted body nodes to represent the soil's reaction forces. Elastic perfectly plastic (t-z) relation for sandy soils, suggested by the American Petroleum Institute [9], is used to represent the nonlinearity of soil springs. An elastic-perfectly plastic model has been used to simulate the pile shaft resistance, [2, 9-12]. It has been also used to model the grout-soil interface in grouted ground anchors [6, 13-15]. As shown in Figure 2, the y axis represents a percent of the mobilized shear stress along with the anchor-soil interface τ to maximum shear stress (τ_{max}), which is calculated by [16]:

$$\tau_{max} = \sigma_v \times K \times \tan \varphi \quad (5)$$

where σ_v is the vertical effective stress, K is the coefficient of lateral earth pressure, and φ is the angle of internal friction of the soil. φ was used instead of the interface angle between the grout and the soil δ , because δ is equal to φ in a good construction method and cast in place concrete to provide a rough grout interface, [17, 18].

The value of K is estimated based on field tests. It ranges from 1 to 2 for coarse silt and fine sand to dense sand and gravel, with grouting pressure less than 10 bar [19]. The stiffnesses of soil springs are added to the global stiffness matrix, as shown in (6):

$$[K]_{global} = [K]_{global} + [K]_{spring} \quad (6)$$

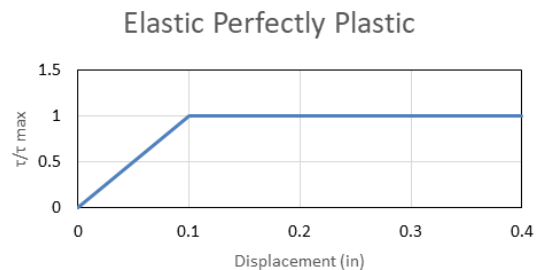


Fig. 2. (t-z) Load transfer relation for sand, (after API, 2005).

B. Grout Modeling

Due to the similarity of the grout material with the concrete material, the stress-strain relation of the concrete under uniaxial compression, suggested by European Standards [20] has been used to model the grouted body under compression. Figure 3 shows the used constitutive model of grout under uniaxial compression. Equations (7)-(13) describe the adopted model.

$$\sigma_c = f_{cm} \left(\frac{k\eta - \eta^2}{1 + (k-2)\eta} \right) \quad (7)$$

$$k = \frac{1.05 \times E_{cm} |\epsilon_{c1}|}{f_{cm}} \quad (8)$$

$$\eta = \frac{\epsilon_c}{\epsilon_{c1}} \quad (9)$$

$$f_{cm}(\text{MPa}) = f_{ck} + 8 \quad (10)$$

$$\epsilon_{cu1}(\%) = 0.35, \text{ for } f_{ck} \leq 50\text{MPa} \quad (11)$$

$$\epsilon_{c1}(\%) = 0.07 \times f_{cm}^{0.31} \leq 0.28\% \quad (12)$$

$$E_{cm} = 22 \left[\frac{f_{cm}}{10} \right]^{0.3} \quad (13)$$

where f_{ck} is the cylinder compression strength at 28 days, in MPa, f_{cm} is the mean of cylinder compressive strength, and all the other parameters are shown in Figure 3.

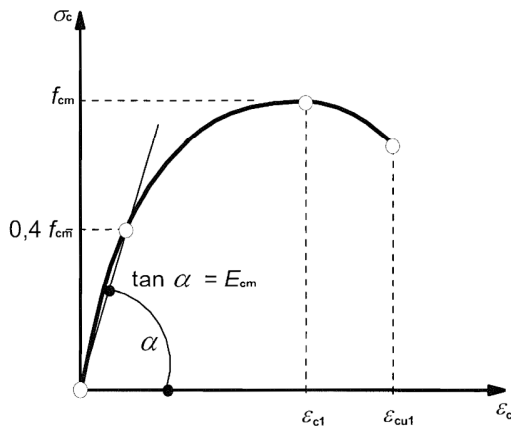


Fig. 3. Constitutive model of grout under compression, (after BS EN 1992-1-1:2004).

A linear elastic constitutive relation has been used to model the grout material under tension stresses before reaching the initial crack. The cracking strain of the grout under tension is about (1×10^{-4}) [21, 22]. The grout stiffness is ignored after reaching the cracking strain.

C. Strand-GROUT Interface Model

The grout-tendon interface is modeled by the local bond stress-slip model for a smooth bar [23], under tension stresses, along the bonded length of the anchor. The adopted model is shown in Figure 4 for smooth bars. Equations (14)-(16) describe the adopted strand-grout interface model.

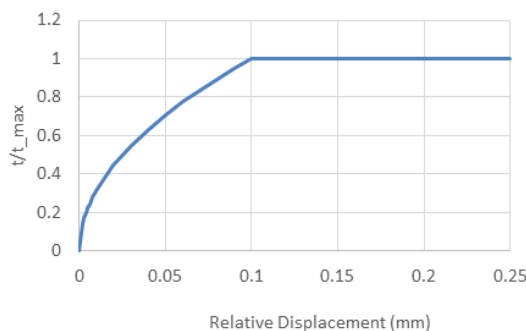


Fig. 4. Local bond stress-slip model for smooth bar, after Ceb Fip, 1990.

$$\tau = \tau_{max} (s/s_1)^\alpha, \text{ for } 0 \leq s \leq s_1 \quad (14)$$

$$\tau = \tau_{max}, \text{ for } s > s_1 \quad (15)$$

$$\tau_{max} = \tau_f = 0.3 \sqrt{f_{ck}} \quad (16)$$

where τ is the shear stress between grout and bar, τ_{max} is the maximum shear stress between the grout and the bar, which is equal to τ_f , which is the residual shear stress after slippage occurs, s is the relative displacement between the grout and the bar, s_1 is the relative displacement at τ_{max} ($s_1=0.1\text{mm}$), f_{ck} is the cube strength of the grout, and $\alpha=0.5$.

The finite element formulation of the strand-grout interface model is made by modifying the applied load vector, according to the relative displacement, and the shear stress between the strand and the grout is calculated according to (14)-(16). The main applied load is reduced by $(\sum_{i=1}^n F_i)$, where n is the number of elements that the slip of the occurred strand-grout interface, and F is the strand-grout interface force which is calculated from:

$$F_i = \tau_i \times A \quad (17)$$

$$A = P_s \times L_{element} \quad (18)$$

$$P_s = m \times \left[\frac{D_s \times \pi \times Num_s}{2} \right] \quad (19)$$

where τ is the shear stress between the strand and the grout, i refers to the number of elements that the slip has occurred, A is the total outside area of all strands surrounding the grout, P_s is the outer perimeter of the strand wires, as shown in Figure 5, $L_{element}$ is element length, m is the number of strands used in the grouted ground anchor, D_s is the diameter of the strand outer single wire, (which is typically equal to 5mm), and Num_s is the number of outer wires in the single strand as illustrated in Figure 5.

Each interface force calculated from (17) is applied to the specified element at the end of each node, and one-half force is applied to each node. The location of the main applied force is changed according to the last element in which the slippage does not occur, i.e. magnitude, number, and location of the applied load are changed according to the bond-slip model between the strand and the surrounding grout, as shown in Figure 6. The interlock between grout and strand group due to using centralizers and spacers ([24]) is neglected.

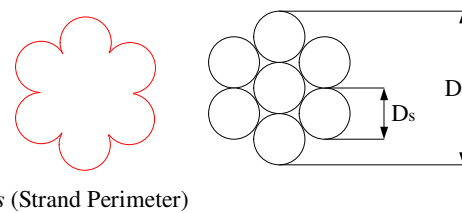


Fig. 5. Section in the strand and outer perimeter of outer wires.

In the case of a compression anchor, there is no connection between the grout and tendon under compression stress (unbonded length of the anchor).

D. Nonlinearity Procedure

The nonlinear behavior of interface spring has been achieved by using the direct iteration method as shown in Figure 7. In this method, the stiffness will be modified in each iteration as described in the algorithm below [25].

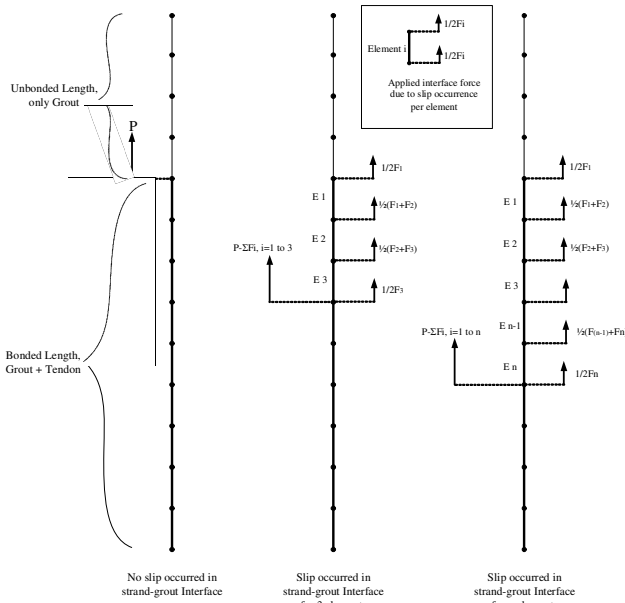


Fig. 6. Change of loads locations and magnitude according to the slip model for tension anchor.

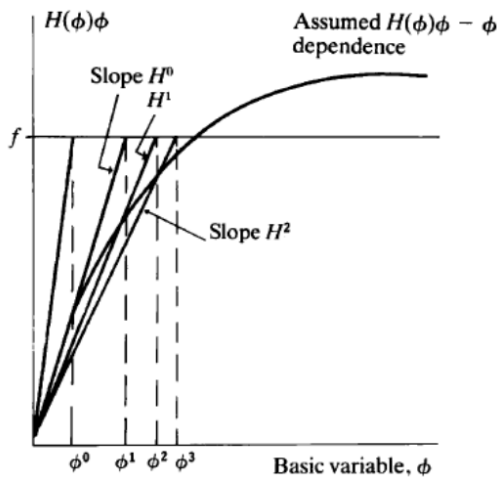


Fig. 7. Direct iteration method.

The following steps illustrate the iteration procedure used to calculate the stiffness of the soil interface, see Figure 8:

- Calculation of the initial stiffness of soil spring using [26]:

$$K_{S_initial} = \frac{2\pi L \bar{G}}{\zeta} \quad (20)$$

where L is the length of the element, \bar{G} is the average shear modulus at the node depth, $\zeta = \ln\left(\frac{2r_m}{d}\right)$, r_m is the max. radius at which soil deformation is very small and it could be neglected, and d is the anchor grouted body diameter.

- Adding the calculated above initial stiffness of soil spring, to the global stiffness matrix, as presented in (6).

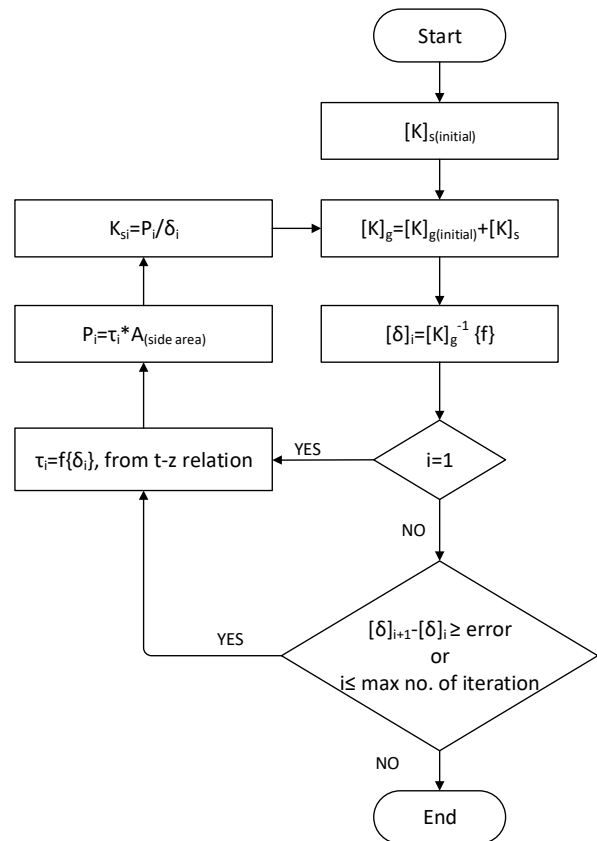


Fig. 8. Flow chart of the iteration loop of soil spring calculation.

- Solving the finite element equation to obtain the nodal displacement (21):

$$\{\delta\}_i = [K]_{global}^{-1} \times \{f\} \quad (21)$$

- Using the nodal displacement obtained in the third step to obtain the shear stress of anchor skin at the node depth from the (t-z) curve. Nodal force is calculated by multiplying the shear stress with the side surface area of the grouted body between the centers of adjacent elements $\{A\}$, as presented in (22):

$$\{f\}_i = \{\tau\}_i \times \{A\} \quad (22)$$

- Calculating a new spring stiffness:

$$[K_{spring}]_i = \{f\}_i / \{\delta\}_i \quad (23)$$

- Adding the calculated spring stiffness to the global stiffness matrix as in (6).
- Repeat steps 3 to 6 to find the nodal displacement $\{\delta\}_{i+1}$.
- Comparing the difference between two successive calculated displacements with the convergence criterion, as in (24):

$$|\{\delta\}_{i+1} - \{\delta\}_i| \leq error \quad (24)$$

As long as the convergence criterion doesn't match, steps 3 to 6 shall be repeated until reaching the maximum number of trials, which have been chosen to be 10^3 .

E. Boundary Conditions

All nodes of the model have one degree of freedom in the vertical direction, which is the direction of the force application and no movements are allowed in the other directions. In the case of an existing structure at the head of the anchor, like the retaining structure or foundation, node no. 1 will be restricted in the vertical direction.

F. Failure Criteria

The failure criteria of the grouted ground anchor are considered below. They take place first in each element, according to the models explained previously:

- Debonding between grout and soil.
- Debonding between grout and tendon.
- Crushing of the grouted body under both tension and compression stresses.
- Tendon failure, by reaching the yield strength of the strand.

G. Development of Algorithms and Verifications

Fortran 90 programming language has been used to code the finite element algorithm, both the pre-processing and equation solver parts, to model the one-dimensional simulation of the ground anchor. Finite element FORTRAN 90 subroutines [27] have been used to build the present finite element algorithm, as described in Table I. Open-source Code Blocks (Release 20.03) IDE platform has been used to compile and run the Fortran finite element code.

TABLE I. FORTRAN 90 SUBROUTINES USED [27]

Subroutine	Purpose
formnf	Forms nodal freedom array
num_to_g	Forms element connectivity vector
fkdiag	Forms the bandwidth vector according to the skyline storage system
rod_km	Forms the stiffness matrix of the rod element
fsparv	Solve the finite element equation system using Cholesky's factorization method
sparin	
spabac	

1) 3-D Plaxis Model Verification

The finite element code has been verified with another finite element solution of grouted ground anchor to verify both the pre-processing and the equation solver. The verification is achieved by using a 3-D finite element model of the ground anchor by PLAXIS software [28]. This model is presented in PLAXIS verification manual for verifications purposes. The properties of the ground anchor model are listed below, as stated in PLAXIS verification manual.

The fixed length is 4m and the free length is 5m, which means that the total length of the anchor is 9m. The strand property is $E_A=4.095 \times 10^3$ kN. The pullout force is estimated to be 752kN [29]. The maximum skin friction along the bonded

length is obtained by dividing the pullout force by the bonded length (188kN/m). The skin friction is assumed to be uniform along the bonded length. Despite this unrealistic assumption, it has been adopted in the developed model for verification purposes. The diameter of the grouted body is 0.125m, with a modulus of elasticity equal to ($E=2.0 \times 10^7$ kN/m²).

The elements used are: 180 bar elements, with equal length of 0.05m. The load-displacement curves of the grouted body proximal end, presented in Figure 9, show very good agreement between the two models. This agreement gives validation for the developed finite element algorithm to be used in the modeling of the grouted ground anchors.

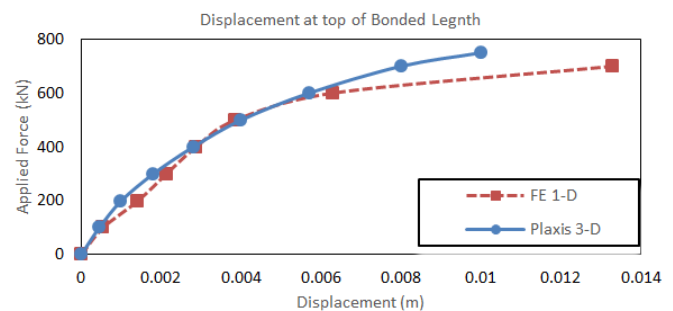


Fig. 9. Load-displacement curves for the proximal end of the verification model of the ground anchor.

2) Field Tests Modeling of the Tension Anchors

The proposed finite element model has been used to simulate pullout tests of three tension-type ground anchors constructed vertically in An-Najaf city in Iraq [30, 31]. The performance test is adopted for all the tested anchors according to the Post Tension Institute [30]. Anchors were trial anchors, they were tested to evaluate their pullout capacity for design purposes. All the tested anchors have a borehole diameter of 150mm and a strand steel area of 560mm². Strain gauges were instrumented along the grouted body of anchor no. (1), therefore, the developed strains were measured, and internal forces were calculated from these measurements. All the tested anchors did not reach failure load which makes the prediction of failure load inaccurate. Instead of that, the safe working load has been determined.

The soil profile and corrected SPT number with depth, for the test site, are shown in Figure 10. The first three trial anchors were installed at the natural ground level, while the other five anchors were installed at 8m below the natural ground. Low grouting pressure was used for grouting all the tested anchors (10kPa=0.1bar) [32]. The properties of tested anchors with the number of elements used for each anchor model are listed in Table II. The modulus of elasticity for the strand is ($E_s=200 \times 10^3$ MPa), while the modulus of elasticity of the grout is calculated according to (25) [33], which is equal to $E_g=22.044 \times 10^3$ MPa.

$$E_g = 4700 \times \sqrt{f_c} \quad (25)$$

TABLE II. PROPERTIES OF TESTED GROUND ANCHORS

Anchor no.	Bonded length (m)	Unbonded length (m)	Unbonded length from the pullout point* (m)	Total embedded length (m)	No. of elements used in the FE models
1	7	3.6	5.2	10.6	212
2	7	5.9	7.2	12.9	258
3	7.5	6	7.3	13.5	270

Figures (11)-(13) show the total displacement of the anchor head vs the applied load for the measured model and the finite element. The displacement consists of the following components:

- Elastic elongation of the tendon free length.
- Elastic displacement of anchor grouted body.
- Plastic displacement of anchor grouted body.

displacement while the calculated one, through the finite element, represents both plastic and elastic components of the anchor head displacement. Through Figures 11-13, a very good agreement could be noticed between the measured and calculated displacement, taking into account that the elastic elongation of the tendon free length represents around (80%) of the total displacement.

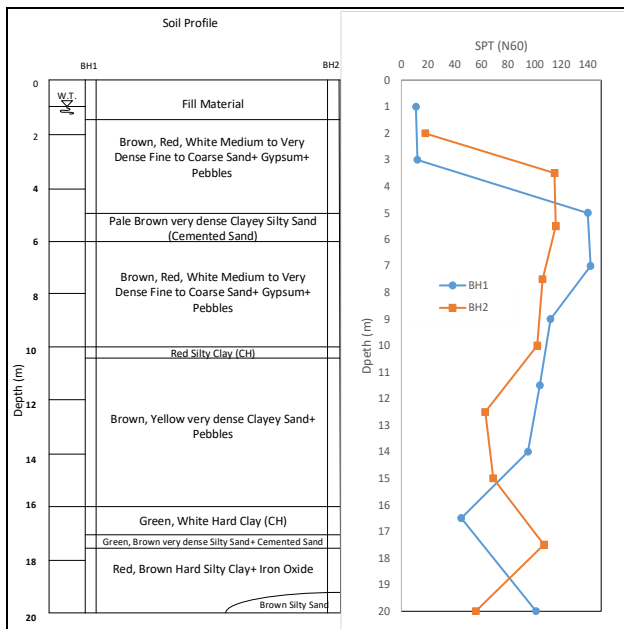


Fig. 10. Soil profile and corrected SPT (N_{60}) values for the test site.

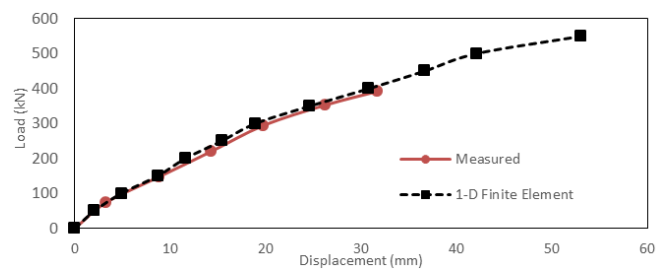


Fig. 12. Load-displacement curves for field test and finite element model anchor (2).

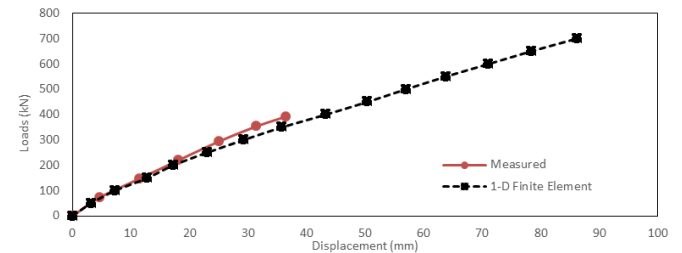


Fig. 13. Load-displacement curves for field test and finite element model anchor (3).

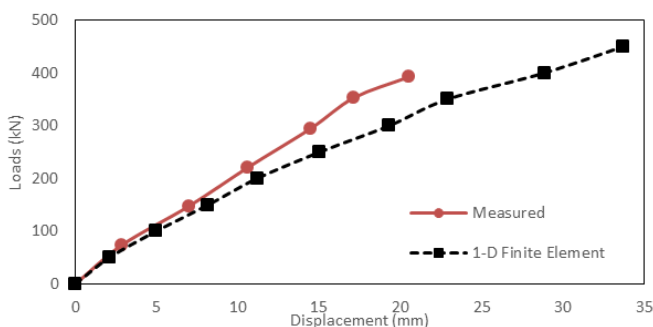


Fig. 11. Load-displacement curves for field test and finite element model anchor (1).

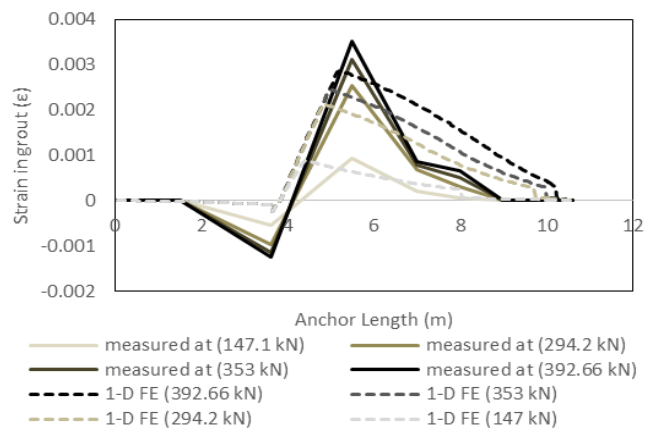


Fig. 14. Strain along the grout of the anchor body.

Comparison with only residual displacement is not possible in the present case, because the measured displacement represents only the plastic component of the anchor head

Figure 14 presents the measured strain along the grout under four loading steps vs the calculated (via finite element modeling) strains. The comparison between the measured and

the calculated strains shows good agreement in the bonded length part with underestimation of the peak point. There is an overestimation of the strain towards the anchor end. On the other hand, the calculated strain is less than the measured strain in the free length part.

III. PARAMETRIC STUDY

According to the previous verifications, the suggested 1-D finite element model is considered reasonably valid for producing parametric studies to investigate some properties of grouted ground anchors.

A. Compression Anchor

A comparative study has been made between compression-type and tension-type anchors, by using the exact data of surrounding soil and anchor properties of trial anchor (1). The applied load in the case of compression anchor is at the lowest node of the anchor's mesh, while it is at the proximal end of the bonded length in the case of tension anchor, as stated in Figure 1. Figure 15 shows the load-displacement curves for both tension and compression anchors. It is noticed that the displacement of the compression-type anchor is less than the half of the displacement of the tension-type one, because the compression stiffness of the grout member is much higher than the tension stiffness. The calculated displacement represents the elastic and plastic components of the anchor head regardless of the elastic elongation of the strand. Both anchors are reached to fully pull out at the same load (400kN), due to the adopted failure modes and grout-soil shear stress distribution as stated in (5).

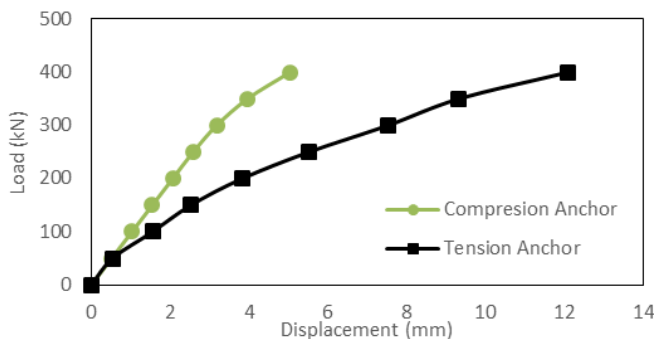


Fig. 15. Load-displacement curves for compression and tension anchor types.

The calculated strains, for both compression and tension anchors, are presented in Figure 16. Obviously, in the tension anchor, the developed strains along the bonded length are tension strains, while its compression strains are along the unbonded length. The maximum value of strain is located at the loading point, at the beginning of the bonded length with shifting towards the anchor toe when the applied load has increased according to the adopted model of debonding between the strand and the grout, see (14)-(16). In the case of a compression anchor, all the developed strains along the anchor body are compression strains. The maximum value of strains is located at the anchor toe, i.e. the loading point, and it decreases until it vanishes at the anchor tip. The tension cracking strain of the grout, which is equal to 1×10^{-4} , has been reached and

exceeded since the 1st loading (100kN) in the case of the tension anchor, while the developed strains did not reach the maximum compression strain of grout (0.003) [34] for the maximum applied load.

A comparison of the mobilized skin friction between tension and compression types is shown in Figure (18). It could be noticed obviously that the compression anchor has a larger maximum mobilized skin friction value than the tension anchor. The distribution of skin friction along the anchor body is not similar for the two types of anchor under consideration, the location of maximum skin friction value is at the anchor toe in the case of compression anchor, while the location of the maximum point is shifted from the proximal end of the bonded length toward the anchor toe with increasing of loading in the case of the tension-type anchor. The total mobilized skin friction force of both types of anchors is approximately equal. The shifting process of skin friction peak point reflects the debonding process between the strand and the grout in bonded length.

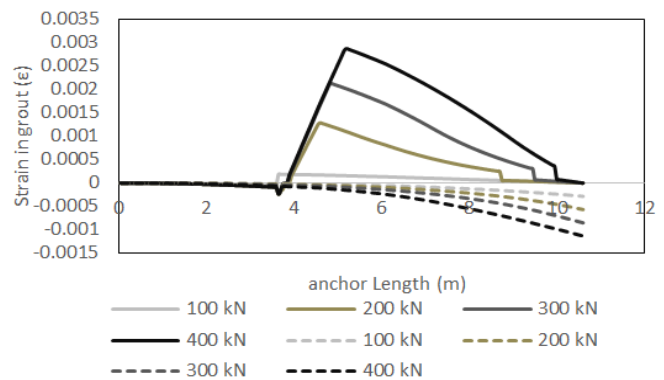


Fig. 16. Strain in the grouted body for compression (dotted line) and tension (continuous line) anchors.

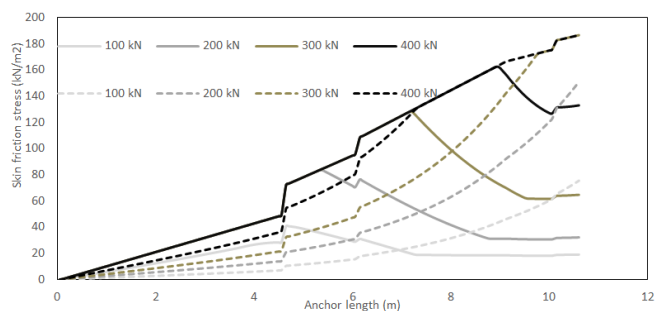


Fig. 17. Skin friction along anchor length, for compression-type (broken line), and tension-type (continuous line).

IV. CONCLUSIONS

A one-dimensional finite element model was developed and used to simulate both tension and compression types of grouted ground anchors. The tendon (steel) grout interface was modeled using the local bond-slip model, while the surrounding soil was modeled using a series of perfectly plastic springs. Verification of the adopted finite element model was made by comparing the results with a three-dimensional finite element model of grouted ground anchor, developed in

PLAXIS, and with the result of field tests of grouted ground anchors. The developed one-dimensional finite element model was used to make a comparison between compression and tension types of grouted ground anchors. From the verification and both comparisons, the following conclusions can be made:

- Load-displacement curves show very good agreement between the developed model and the finite element three-dimensional model, showing very good agreement with the filed test result. The comparison between the calculated and measured strains in the field test results shows some differences along the unbonded length part, but with good agreement in the bonded length part.
- The displacement of anchor head is smaller in the case of compression anchor, which makes it bear high design load.
- The developed strain in the grouted body of the compression anchor is much smaller than the tension-type, which means less cracking in the grouted body providing additional corrosion protection.

REFERENCES:

- [1] C. S. Desai and T. Kuppusamy, "Application of a numerical procedure for laterally loaded structures," in *Numerical methods in offshore piling*, Atlanta, GA, USA: ICE Publishing, 1980, pp. 93–99.
- [2] M. Georgiadis, "Interaction between torsional and axial pile responses," *International Journal for Numerical and Analytical Methods in Geomechanics*, vol. 11, no. 6, pp. 645–650, 1987, <https://doi.org/10.1002/nag.1610110609>.
- [3] C. S. Desai and M. Zaman, *Advanced Geotechnical Engineering: Soil-Structure Interaction using Computer and Material Models*. Boca Raton, FL, USA: CRC Press, 2013.
- [4] H. J. Seo and L. Pelecanos, "Finite element analysis of soil-structure interaction in soil anchor pull-out tests," in *Numerical Methods in Geotechnical Engineering IX*, Boca Raton, FL, USA: CRC Press, 2018.
- [5] H. J. Seo, G. Marketos, and L. Pelecanos, "Soil-structure interaction in field pull-out tests of soil anchors and additional resistance from the reaction plate," in *XVII European Conference on Soil Mechanics and Geotechnical Engineering*, Reykjavik, Iceland, Sep. 2019, pp. 1–8.
- [6] J. Smet, N. Huybrechts, G. V. Lysebetten, J. Verstraelen, and S. François, "Optical Fiber Strain Measurements and Numerical Modeling of Load Tests on Grouted Anchors," *Journal of Geotechnical and Geoenvironmental Engineering*, vol. 145, no. 12, Dec. 2019, Art. no. 04019103, [https://doi.org/10.1061/\(ASCE\)GT.1943-5606.0002167](https://doi.org/10.1061/(ASCE)GT.1943-5606.0002167).
- [7] T. S. Phan, P. Rossi, and J.-L. Tailhan, "Numerical modelling of the concrete/rebar bond," *Cement and Concrete Composites*, vol. 59, pp. 1–9, May 2015, <https://doi.org/10.1016/j.cemconcomp.2015.02.003>.
- [8] A. Spada, G. Giambanco, and P. Rizzo, "Elastoplastic Damaging Model for Adhesive Anchor Systems. I: Theoretical Formulation and Numerical Implementation," *Journal of Engineering Mechanics*, vol. 137, no. 12, pp. 854–861, Dec. 2011, [https://doi.org/10.1061/\(ASCE\)EM.1943-7889.0000287](https://doi.org/10.1061/(ASCE)EM.1943-7889.0000287).
- [9] *Recommended Practice for Planning, Designing and Constructing Fixed Offshore Platforms—Working Stress Design*. Washington DC, USA: American Petroleum Institute, 2005.
- [10] E. Motta, "Approximate Elastic-Plastic Solution for Axially Loaded Piles," *Journal of Geotechnical Engineering*, vol. 120, no. 9, pp. 1616–1624, Sep. 1994, [https://doi.org/10.1061/\(ASCE\)0733-9410\(1994\)120:9\(1616\)](https://doi.org/10.1061/(ASCE)0733-9410(1994)120:9(1616)).
- [11] D. A. Mangnejo, S. J. Oad, S. A. Kalhor, S. Ahmed, F. H. Laghari, and Z. A. Siyal, "Numerical Analysis of Soil Slope Stabilization by Soil Nailing Technique," *Engineering, Technology & Applied Science Research*, vol. 9, no. 4, pp. 4469–4473, Aug. 2019, <https://doi.org/10.48084/etasr.2859>.
- [12] P. H. V. Nguyen and P. C. Nguyen, "Effects of Shaft Grouting on the Bearing Behavior of Barrette Piles: A Case Study in Ho Chi Minh City," *Engineering, Technology & Applied Science Research*, vol. 11, no. 5, pp. 7653–7657, Oct. 2021, <https://doi.org/10.48084/etasr.4389>.
- [13] K. Fujita, K. Ueda, and M. Kusabuka, "A method to predict the load-displacement relationship of ground anchors," *Revue Francaise de Geotechnique*, no. 3, pp. 58–62, 1978, <https://doi.org/10.1051/geotech/1978003058>.
- [14] N.-K. Kim, "Performance of Tension and Compression Anchors in Weathered Soil," *Journal of Geotechnical and Geoenvironmental Engineering*, vol. 129, no. 12, pp. 1138–1150, Dec. 2003, [https://doi.org/10.1061/\(ASCE\)1090-0241\(2003\)129:12\(1138\)](https://doi.org/10.1061/(ASCE)1090-0241(2003)129:12(1138)).
- [15] N.-K. Kim, J.-S. Park, and S.-K. Kim, "Numerical simulation of ground anchors," *Computers and Geotechnics*, vol. 34, no. 6, pp. 498–507, Nov. 2007, <https://doi.org/10.1016/j.compgeo.2006.09.002>.
- [16] P. Moller and S. Widing, "Anchoring in soil employing the Alvik, Lindo and JB drilling methods," in *7th International Conference for Soil Mechanics and Foundation Engineering*, 1969, vol. 15.
- [17] H.-Y. Fang, Ed., *Foundation Engineering Handbook*, 2nd ed. 1991. Softcover reprint of the original 2nd ed. 1991 edition. New York, NY, USA: Springer, 2012.
- [18] J. G. Potyondy, "Skin Friction between Various Soils and Construction Materials," *Geotechnique*, vol. 11, no. 4, pp. 339–353, Dec. 1961, <https://doi.org/10.1680/geot.1961.11.4.339>.
- [19] G. S. Littlejohn, "Design estimation of the ultimate load-holding capacity of ground anchors," *Ground Engineering*, vol. 13, no. 8, pp. 25–39, Nov. 1980.
- [20] *BS EN 1992-1-1(2004), Design Of Concrete Structures. General Rules And Rules For Buildings*. London, UK: British Standards Institution, 2004.
- [21] F. Leonhardt, "Cracks and crack control at concrete structures," in *International Association for Bridge and Structural Engineering*, Versailles, Paris, France, Sep. 1987.
- [22] J.-L. Briaud, W. F. P. Iii, and D. E. Weatherby, "Should Grouted Anchors Have Short Tendon Bond Length?," *Journal of Geotechnical and Geoenvironmental Engineering*, vol. 124, no. 2, pp. 110–119, Feb. 1998, [https://doi.org/10.1061/\(ASCE\)1090-0241\(1998\)124:2\(110\)](https://doi.org/10.1061/(ASCE)1090-0241(1998)124:2(110)).
- [23] *Committee Euro-International du Beton, CEB-FIP Model Code 1990*. London, UK: Thomas Telford Publishing, 1990.
- [24] *Federal Highway Administration, Geotechnical Engineering Circular No. 4, Ground Anchors and Anchored Systems*. Washington, DC, US: US Department of Transportation, 1999.
- [25] A. D. Booth, *Numerical methods*, 3rd ed. Oxford, UK: Butterworths, 1966.
- [26] M. F. Randolph and C. P. Wroth, "Analysis of Deformation of Vertically Loaded Piles," *Journal of the Geotechnical Engineering Division*, vol. 104, no. 12, pp. 1465–1488, Dec. 1978, <https://doi.org/10.1061/AJGEB6.0000729>.
- [27] I. M. Smith and D. V. Griffiths, *Programming the Finite Element Method*. New York, NY, USA: John Wiley & Sons, 2004.
- [28] *Plaxis Manual of Verification and Validation*, Bentley Systems Inc., 2018.
- [29] *U. Smolczyk, Geotechnical Engineering Handbook, Procedures*. Berlin, Germany: John Wiley & Sons, 2003.
- [30] N. H. Al-Baghdadi and B. A. Ahmed, "Field Tests of Grouted Ground Anchors in Sandy Soil of Najaf, Iraq," *Open Engineering Journal*, accepted for publishing on 19 July 2022.
- [31] E. M. Kara, M. Meghachou, and N. Aboubekr, "Contribution of Particles Size Ranges to Sand Friction," *Engineering, Technology & Applied Science Research*, vol. 3, no. 4, pp. 497–501, Aug. 2013, <https://doi.org/10.48084/etasr.361>.
- [32] *PTI DC35(2014), Recommendations for Prestressed Rock and Soil Anchors*. Post Tensioning Institute, 2014.
- [33] P. Xanthakos, *Ground Anchors and Anchored Structures*. New York, NY, USA: John Wiley & Sons, 1991.
- [34] *ACI 318-(2019), Building Code Requirements for Structural Concrete and Commentary*. Farmington Hills, MI, USA: ACI Concrete, 2019.